Observations of the sensitivity of beam attenuation to particle size in a coastal bottom boundary layer

P. S. Hill,[1] E. Boss,[2] J. P. Newgard,[1] B. A. Law,[3] and T. G. Milligan[3]

Received 21 July 2010; revised 3 November 2010; accepted 2 December 2010; published 16 February 2011.

[1] The goal of this study was to test the hypothesis that the aggregated state of natural marine particles constrains the sensitivity of optical beam attenuation to particle size. An instrumented bottom tripod was deployed at the 12-m node of the Martha's Vineyard Coastal Observatory to monitor particle size distributions, particle size-versus-settling-velocity relationships, and the beam attenuation coefficient (c_p) in the bottom boundary layer in September 2007. An automated in situ filtration system on the tripod collected 24 direct estimates of suspended particulate mass (*SPM*) during each of five deployments. On a sampling interval of 5 min, data from a Sequoia Scientific LISST 100x Type B were merged with data from a digital floc camera to generate suspended particle volume size distributions spanning diameters from approximately 2 μm to 4 cm. Diameter-dependent densities were calculated from size-versus-settling-velocity data, allowing conversion of the volume size distributions to mass distributions, which were used to estimate SPM every 5 min. Estimated *SPM* and measured c_p from the LISST 100x were linearly correlated throughout the experiment, despite wide variations in particle size. The slope of the line, which is the ratio of c_p to *SPM*, was 0.22 g m^{-2}. Individual estimates of c_p:*SPM* were between 0.2 and 0.4 g m^{-2} for volumetric median particle diameters ranging from 10 to 150 μm. The wide range of values in c_p:*SPM* in the literature likely results from three factors capable of producing factor-of-two variability in the ratio: particle size, particle composition, and the finite acceptance angle of commercial beam-transmissometers.

Citation: Hill, P. S., E. Boss, J. P. Newgard, B. A. Law, and T. G. Milligan (2011), Observations of the sensitivity of beam attenuation to particle size in a coastal bottom boundary layer, *J. Geophys. Res.*, *116*, C02023, doi:10.1029/2010JC006539.

1. Introduction

[2] Suspended particulate mass (*SPM*) in natural waters affects a variety of processes. It can block light, smother organisms living on the seabed, transport particle-attached contaminants, and degrade the aesthetics of coastal waters [e.g., *Smith et al.*, 1995; *Moore et al.*, 1997; *Santschi et al.*, 1997; *Fabricius and Wolanski*, 2000]. Long, high-resolution time series of directly measured *SPM* are desirable due to the high frequency and episodic nature of SPM variability, yet they are not practical to assemble because of the substantial time and labor required to measure *SPM* directly. Water must be collected, and then the particles must be filtered and weighed. The need to know suspended sediment concentration, paired with the difficulty of measuring it directly, has led to the development of instruments that link water column optical properties to *SPM*. Unfortunately, since their invention, optical instruments have been undermined by concerns regarding sensitivity to particle size [e.g., *Downing*, 2006].

[3] Optical instruments were developed in large part to permit continuous, remote, in situ sensing of suspended particulate mass over a range of forcing conditions. Ironically, this goal was motivated partly by the knowledge that particle size can change dramatically in response to forcing by waves and currents, which, according to theory based on solid spheres, makes the conversion from optical properties to *SPM* uncertain [e.g., *Baker and Lavelle*, 1984]. A recent model of the optical properties of suspensions of natural particles, however, proposes that because many marine particles are aggregates, sensitivity of optical properties to particle size may be constrained [*Boss et al.*, 2009b]. The goal of this paper is to use in situ measurements to examine this hypothesis.

2. Background

[4] Particles suspended in water attenuate light, either by absorbing it or by scattering it. The interaction of light and particles in water is complex, but when a suspension is dilute and the positions of particles are random and time-varying, which is an accurate description of many marine particle suspensions, attenuation caused by a group of particles can be found simply by summing the contributions of individual

[1]Department of Oceanography, Dalhousie University, Halifax, Nova Scotia, Canada.
[2]School of Marine Sciences, University of Maine, Orono, Maine, USA.
[3]Fisheries and Oceans Canada, Bedford Institute of Oceanography, Dartmouth, Nova Scotia, Canada.

Copyright 2011 by the American Geophysical Union.
0148-0227/11/2010JC006539

particles [*van de Hulst*, 1981]. Alternatively, light attenuation can be measured to extract information about the concentration of suspended particles. This is a common application of beam transmissometers.

[5] Transmissometers measure the drop in intensity of a nearly monochromatic light beam as it traverses a fixed distance. The drop in intensity is converted to a particulate beam attenuation coefficient with the equation [e.g., *van de Hulst*, 1981]

$$c_p = \frac{\ln\left(J_o/J\right)}{L} \tag{1}$$

where J_o is the intensity of light measured in a volume of particle-free water (cd), J is the measured intensity in the presence of particles (cd), and L (m) is the path length over which the transmitted beam travels (see Notation section). Note that equation (1) actually defines the beam attenuation coefficient due to both particles and dissolved substances in the water and that the attenuation due to water is removed by comparing measured intensity to intensity in particle-free water. Because commercial transmissometers measure optical attenuation at wavelengths of light minimally affected by attenuation by dissolved substances [cf. *Bricaud et al.*, 1981], however, the measured attenuation coefficient is typically equated to the particulate beam attenuation coefficient. This coefficient, c_p, has units of m^{-1} and can be linked to particle properties by summing the individual contributions of all particles to attenuation.

[6] Attenuation due to a single particle of diameter D is represented by the product of a diameter-dependent dimensionless attenuation efficiency, $Q_c(D)$, and the geometric cross section of the particle. The attenuation per unit of volume of water due to all particles on the size interval D to $D + dD$ is found by multiplying the attenuation due to a single particle of that size by $n(D)$, which is the number concentration per unit of volume between D and $D + dD$. The variable $n(D)$ has units of number per unit volume per diameter increment, or m^{-4}. Attenuation due to all particles in a suspension is found by integrating over the entire range of particle sizes:

$$c_p = \int_{D_{\min}}^{D_{\max}} Q_c(D) n(D) \frac{\pi D^2}{4} dD. \tag{2}$$

The variables $D_{\min}$ and $D_{\max}$ are the smallest and largest particle sizes found in a suspension. The values of $D_{\min}$ and $D_{\max}$ are not well defined and vary among environments [e.g., *Yamasaki et al.*, 1998; *Mikkelsen et al.*, 2006]. Submicrometer particles are abundant in the ocean, with concentrations linked to biological activity. It is not clear the degree to which these particles exist as independent entities or within aggregates of many particles [*Yamasaki et al.*, 1998]. As a result, the definition of $D_{\min}$ remains an operational one. Maximal particle size is affected by resuspension, particle aggregation and disaggregation, sedimentation, and advection [*Mikkelsen et al.*, 2006]. Its definition also is often operational or based on in situ observations.

[7] The conversion of beam attenuation coefficient to *SPM* is achieved by substituting an expression that contains suspended mass concentration on the interval D to $D + dD$ ($m(D)$)for $n(D)$ in equation (2). The units of $m(D)$ are g m^{-4}. Suspended number concentration may be written in terms of suspended mass concentration by dividing the latter by the mass of an individual particle of diameter D:

$$n(D) = \frac{m(D)}{\rho_s(D)\pi D^3/6}. \tag{3}$$

The term $\rho_s(D)$ is the density of a particle of diameter D (g m^{-3}). The dependence of c_p on suspended sediment concentration can be clarified by defining a mass frequency distribution, $f_m(D)$, which is simply the suspended mass concentration of particles of diameter D divided by the total suspended mass concentration:

$$f_m(D) = \frac{m(D)}{\int_{D_{\min}}^{D_{\max}} m(D)dD} = \frac{m(D)}{SPM} \tag{4}$$

By substituting equation (3) into equation (2) and rewriting the mass concentration as the product of SPM and $f_m(D)$ (equation (4)), an expression for attenuation as a function of suspended particulate mass results:

$$c_p = SPM \int_{D_{\min}}^{D_{\max}} Q_c(D) \frac{3 f_m(D)}{2\rho_s(D)D} dD. \tag{5}$$

Equation (5) demonstrates that attenuation of light by particles will be directly proportional to suspended particulate mass only if the shape of the particle size distribution, which is described by the frequency distribution $f_m(D)$, the maximum and minimum particle sizes, the attenuation efficiency, and the particle density are constant. In practice, the variables in the integral are not known a priori nor are they expected to be the same in different suspensions, so a calibration is carried out in which measured attenuation coefficients are regressed on measured *SPM* to obtain the value of the integral. This value is referred to either as the c_p:*SPM* ratio or the mass-normalized beam attenuation coefficient, c_{p*}. In this paper, the former will be used. The units of c_p:*SPM* are m^2 g^{-1}, demonstrating that this ratio expresses the optical cross section per unit mass of particles in suspension.

[8] Numerous studies reveal a range in the values of c_p:*SPM* that extends over an order of magnitude from as low as 0.05 to as high as 1.5 (Figure 1). The most obvious candidate for causing this range of values is variable particle size in suspension, which can vary by over two orders of magnitude in natural bottom-boundary layer suspensions [e.g., *Mikkelsen et al.*, 2006]. A useful way to illustrate the potential sensitivity of c_p:*SPM* to size is to consider a suspension composed of spheres of a single diameter. Under this assumption, c_p:*SPM* simplifies considerably:

$$c_p : SPM = \frac{3Q_c(D)}{2\rho_s(D)D}. \tag{6}$$

For solid spheres of identical composition and density, and diameters much larger than the wavelength of light, all terms in equation (6) are constant except for D [*van de Hulst*, 1981]. Under these circumstances this equation shows that

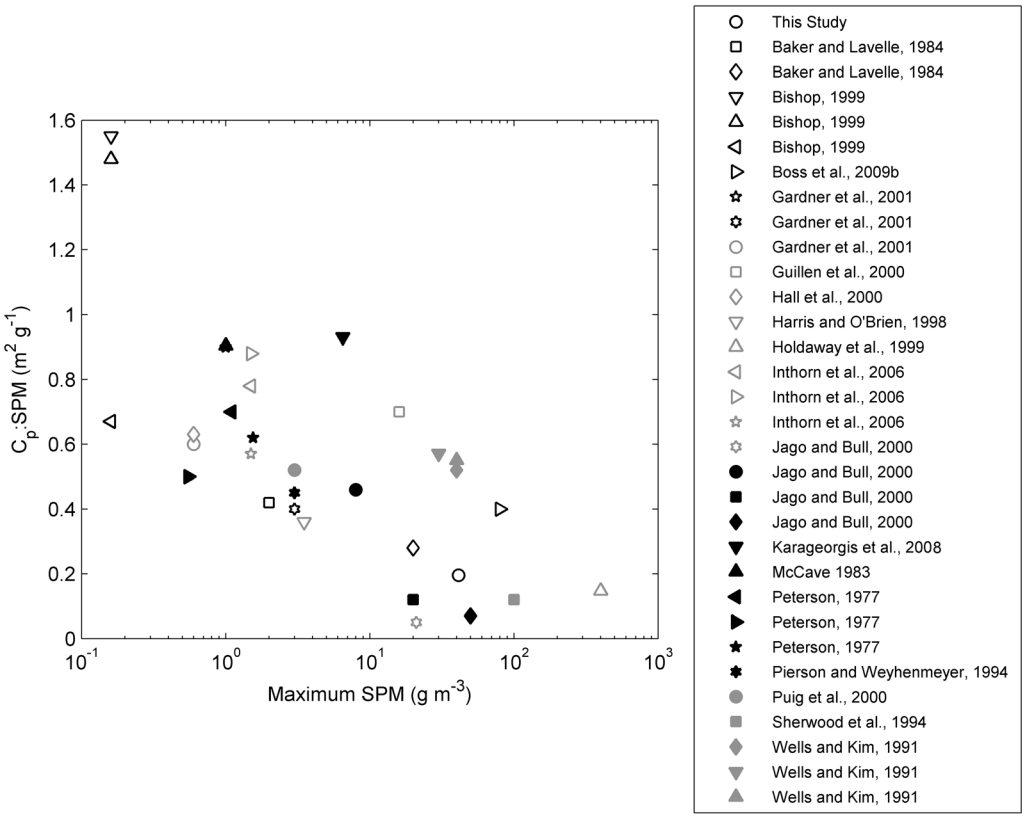

Figure 1. Literature values of c_p:*SPM* plotted versus the maximum reported suspended sediment concentration during the study. Note the general decrease in c_p:*SPM* as maximum reported *SPM* increases. This decrease is similar to the one reported by *Baker and Lavelle* [1984] as measurements moved from deep to shallow water. The choice to plot c_p:*SPM* versus the maximum reported suspended sediment concentration was a practical one because maximal sediment concentration typically is reported in studies, whereas water depth at site of measurement is not always reported, particularly in pelagic studies. Furthermore, *Baker and Lavelle* [1984] argue that the trend of decreasing c_p:*SPM* with decreasing water depth reflects increasing energy in shallower waters, which in turn causes elevated sediment concentrations and larger particle sizes.

c_p:*SPM* is inversely proportional to the diameter of the spheres in suspension. Small particles, which are still large relative to the wavelength of light, attenuate more light per unit of mass than large particles because they have larger surface to volume ratios. To explain an order of magnitude variability in c_p:*SPM* simply requires a similar range in particle size [*Baker and Lavelle*, 1984; *Wiberg et al.*, 1994; *Bunt et al.*, 1999; *Mikkelsen*, 2002]. Observations of suspended particle size distributions in bottom boundary layers show that such a range in variability is typical, with *Mikkelsen et al.* [2006], for example, observing a range in median suspended particle diameter in Adriatic bottom boundary layers of 17–2800 μm. Acceptance of size variation as the underlying cause of the observed variability in c_p:*SPM*, however, undermines confidence in the applicability of attenuation as a proxy for suspended sediment mass [e.g., *Fugate and Friedrichs*, 2002]. In short, variability in attenuation caused by changes in particle size can be of similar magnitude to variability caused by changes in suspended particulate mass. Without independent measurements of particle size, assigning variations in attenuation to mass or size is not possible [*Mikkelsen and Pejrup*, 2000]. Despite this potentially profound problem, transmissometers continue to be a reasonably accurate tool for estimating suspended sediment concentration [e.g., *Bunt et al.*, 1999; *Mikkelsen and Pejrup*, 2000; *Boss et al.*, 2009c].

[9] In a study commissioned by the Alliance of Coastal Technologies (ACT), *Boss et al.* [2009c] compared colocated measurements of the beam attenuation coefficient and *SPM*. The ACT data set was collected from moored deployments at eight test sites representing a range of environmental conditions including a tropical coral reef, a high turbidity estuary, the open ocean, and a freshwater lake. Beam attenuation and *SPM* both ranged over two orders of magnitude in the combined data set. The fraction of organic to total mass also varied among the sites. Particle size was not quantified, but the diversity of environments likely produced a range in size distributions. Despite observed and presumed variability in the factors that define c_p:*SPM*, the relationship between beam attenuation and SPM was constrained, with 95% of values of *SPM* predicted from c_p falling within 54% of the measured SPM. This factor of 2 range of variability is much smaller than equation (6) would suggest based on expected variability in particle size. This scale of variability in c_p:*SPM* has been found by others in environments where particle size is variable [*Bunt et al.*, 1999; *Mikkelsen and Pejrup*, 2000].

[10] Particle aggregation offers a mechanism for resolving the paradox of small variability in c_p:*SPM* in the presence of large variability in particle size. In natural waters particles clump to form aggregates, which are also referred to as flocs. Aggregates form where conditions produce encounters between particles in suspension and when there is a mechanism to make colliding particles stick. Particles encounter one another due to turbulent shear, differential settling, and Brownian motion [cf. *McCave*, 1984], with moderate turbulence favoring frequent collisions, but energetic turbulence leading to aggregate breakup [cf. *Winterwerp and van Kesteren*, 2004]. Cohesion of particles can be mediated electrochemically via compression of ionic electrical double layers around charged particles in water with salinities above a few parts per thousand. Alternatively, adhesion can occur via organic bridging between particles [cf. *Hill et al.*, 2007].

[11] Early in the study of aggregates, it was recognized that aggregate density is a decreasing function of aggregate size, indicating that mass scales as diameter raised to a power less than 3 [e.g., *McCave*, 1984]. The relationship between diameter and mass subsequently was described in terms of fractal geometry, for which the mass of a particle scales with diameter raised to an exponent known as the fractal dimension, F [e.g., *Orbach*, 1986]:

$$\rho_a(D)\frac{\pi D^3}{6} \propto D^F. \quad (7)$$

In equation (7) $\rho_a(D)$ is the density of an aggregate of diameter D. The value of F typically is determined by measuring in situ size-versus-settling-velocity relationships and then solving for the density required to produce the observed settling velocity for an aggregate of size D. The log of density is then regressed on the log of diameter to produce an estimate of F [*Hill et al.*, 1998; *Sternberg et al.*, 1999; *Fox et al.*, 2004]. Rewriting equation (7) in terms of aggregate density indicates that it is proportional to $D^{(F-3)}$. Values of F near 2 are common, meaning that density of an aggregate scales approximately with the inverse of aggregate diameter.

[12] Substitution into equation (5) of an expression for aggregate density that assumes $F = 2$ produces an interesting result:

$$c_p : SPM \propto \int_{D_{\min}}^{D_{\max}} \frac{Q_c(D) f_m(D)}{D^{-1}D} dD \propto \int_{D_{\min}}^{D_{\max}} Q_c(D) f_m(D) dD, \quad (8)$$

where constants have been dropped for convenience. This equation can be simplified further by noting that, because marine aggregates are much larger than the wavelength of light, $Q_c(D)$ is approximately equal to 2 [*van de Hulst*, 1981]. So, for a suspension in which the majority of mass is in aggregates, c_p:*SPM* does not depend on diameter because the integral of the mass frequency distribution over all particle sizes is, by definition, equal to unity (equation (4)).

[13] The theoretical result that c_p:*SPM* is not dependent on diameter if $F = 2$ has been noted by several authors [*Hill et al.*, 1994; *Hatcher et al.*, 2001; *Ganju et al.*, 2006; *Curran et al.*, 2007]. This relatively simple analysis was extended by *Nikora et al.* [2004] to argue that aggregates with fractal dimensions less than or equal to 2 rendered optical properties insensitive to particle size. *Berry and Percival*'s [1986] work on aggregates in smoke can be interpreted similarly. For aggregates with fractal dimensions less than 2, the optical cross section of an aggregate is proportional to the sum of the optical cross sections of its component particles, so packaging of individual particles into aggregates does not affect the overall optical properties of the suspension.

[14] These arguments are illustrative, but perhaps too simplistic, because they do not address the likelihood that marine aggregates are not true fractals, with one fractal dimension that describes the entire size distribution [*Khelifa and Hill*, 2006; *Maggi*, 2007]. Instead, smaller aggregates likely have larger "fractal dimensions" than larger aggregates. *Boss et al.* [2009b] incorporated more realistic descriptions of particle geometry into an optical model of aggregates and applied it to a range of idealized, power law size distributions. This theoretical work showed that the relative insensitivity of c_p:*SPM* to particle size persists. Another potential limitation of the theoretical work is the use of power law size distributions, for which concentration is a monotonic function of size. Natural distributions of particle volume typically possess a distinct mode and at times are observed to be bimodal [e.g., *Mikkelsen et al.*, 2007]. Such distributions may also affect the sensitivity of c_p:*SPM* to variations in particle size. Therefore, to test the hypothesis that the relative size invariance of c_p:*SPM* is due to the fractal geometry of natural aggregates, this study was designed to gather simultaneous, in situ measurements of attenuation, *SPM*, and particle size distribution over a range of forcing conditions in a coastal bottom boundary layer.

3. Methods

[15] The Modified in Situ Size and Settling Column Tripod (MINSSECT) was deployed to measure c_p, *SPM* and particle size distributions. The MINSSECT is the successor to the INSSECT [*Mikkelsen et al.*, 2004], carrying the same basic set of instrumentation on a different frame. MINSSECT has a Sequoia Scientific LISST 100x Type B laser particle sizer and a Digital Floc Camera (DFC) to measure a range of particle diameters from approximately 2 μm to 4 cm. The LISST also measures the beam attenuation coefficient, c_p. Size-versus-settling-velocity measurements are made with a digital video camera that images a slab of fluid in a settling column. These measurements are used to estimate particle density as a function of particle size, which in turn allows estimation of SPM based on particle size distributions measured with the LISST and DFC. A new addition to the MINSSECT is an in situ water filtration system (McLane Research Laboratories, Inc. Phytoplankton Sampler). With this system, the accuracy of the conversion from suspended volume to suspended mass can be evaluated by comparing estimated and observed SPM. All instruments were mounted so the centers of the measuring volumes were located 1.2 m above the seabed.

[16] MINSSECT was deployed at the 12-m offshore node of the Woods Hole Oceanographic Institution's Martha's Vineyard Coastal Observatory (MVCO) [*Edson et al.*, 2001]. The facility is located on the south coast of Martha's Vineyard, along a relatively straight 25-km stretch of sandy coastline that faces the open ocean to the south. The MVCO includes a small shore lab, a 10-m meteorological mast, a subsurface node mounted in 12-m water depth approximately 1.5 km offshore, and an air-sea interaction tower (ASIT) at

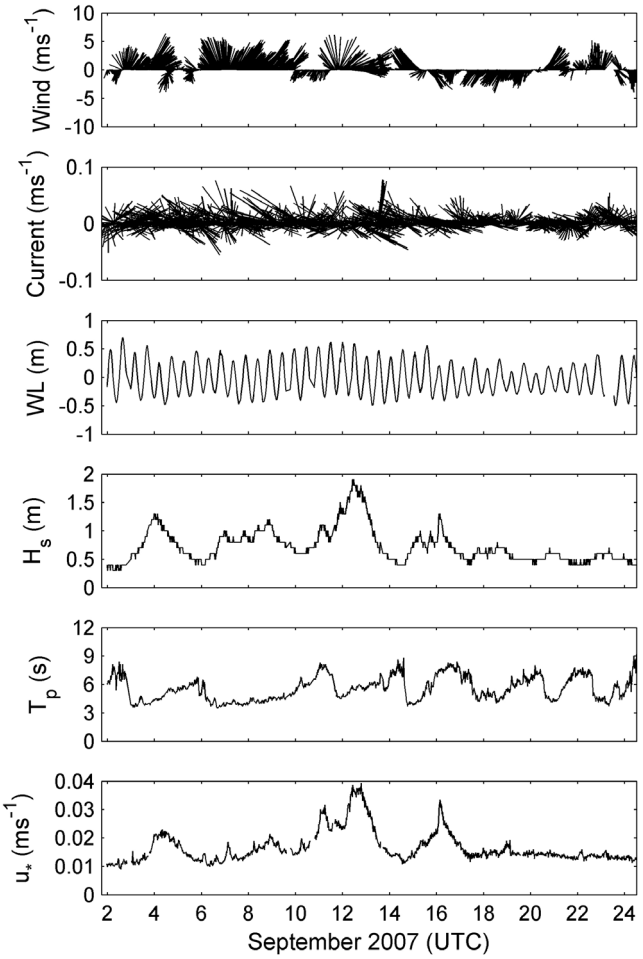

Figure 2. Forcing at Martha's Vineyard Coastal Observatory during the 2007 deployment period. From top to bottom are shown wind velocity, current velocity, water level, significant wave height, dominant wave period, and estimated combined wave plus current shear velocity. Positive wind and current velocities are associated with flow from south to north.

the 15-m isobath. The meteorological and subsea instrumentation are connected directly to the shore lab via a buried electro-optic power cable. The core set of instruments at the meteorological mast measure wind speed and direction, temperature, humidity, precipitation, CO_2, solar and IR radiation, momentum, heat, and moisture fluxes. The core oceanographic sensors at the 12-m offshore node measure current profiles, waves, temperature, salinity, and near-bottom wave-orbital velocity and low-frequency currents.

[17] Five deployments of the MINSSECT occurred in September 2007. The first extended from 1 to 2 September, the second from 2 to 9 September, the third from 10 to 13 September, the fourth from 13 to 19 September, and the fifth from 20 to 24 September. To minimize the effects of biofouling, windows of the LISST and the cameras were cleaned between each deployment. During the deployments, prevailing winds were from the south (Figure 2), with periods of southerly winds separated by several days of northerly winds. The periods of northerly winds generally were associated with long, low-amplitude swell, while southerly winds produced shorter period, larger waves that reached significant wave heights near 2 m. September was chosen as the deployment month because of the range of forcing conditions typical of this time of year.

[18] The LISST estimated the volume concentration of particles with diameters in the range 1.25–250 μm at 5-min intervals. The LISST measured the intensity of light (670 nm) scattered by particles onto 32 logarithmically spaced ring detectors. It also measured how much light was transmitted across its 5-cm path length. The pattern of scattered light was inverted into a particle size distribution using an instrument-specific calibration of the scattering pattern of particles of known size and volume concentration [*Traykovski et al.*, 1999; *Agrawal and Pottsmith*, 2000; *Mikkelsen et al.*, 2005]. The distribution was divided into 32 logarithmically spaced size bins with diameter midpoints of the bins ranging from 1.36 to 230 μm, herein referred to as bins 1–32. Assuming spherical geometry, the particle size distributions were converted to area and volume distributions. Sequoia Scientific's spherical scattering property kernel matrix, as opposed to the recently developed random-shape matrix, was used to invert the data. The ratio of the intensity of the transmitted light in a sample to the intensity of light transmitted through a chamber of particle-free water was used to calculate the attenuation coefficient, c_p (equation (1)). This method removes attenuation due to water. Attenuation due to dissolved substances is minimized by using a wavelength (670 nm) for which absorption by these substances is small [*Bricaud et al.*, 1981].

[19] A digital floc camera (DFC) [*Mikkelsen et al.*, 2004] captured silhouette still images of suspended particles every 5 min, coincident with the LISST. The field of view was a 4 × 4 × 2.5-cm slab of water that flowed between two glass plates. The pixel size of the DFC is ~15 μm. To be considered a particle, objects were required to comprise a minimum of 9 pixels, so the smallest particle that was resolved was approximately 45 μm in diameter (3 × 3 pixels). For each deployment, an area of interest (AOI) was chosen to analyze only the best portion of the images, minimizing the interference of quasi-stationary debris on the glass plates. The color images were cropped to the AOI, transformed to gray scale, and processed using a top-hat filter to smooth the background pixel intensity [*Gonzalez et al.*, 2004]. For each image, the threshold gray scale value, used to define particle edges from the image background, was defined using Otsu's method [*Otsu*, 1979]. The particle areas in each image were converted to equivalent spherical volumes and apportioned into 35 logarithmically spaced diameter bins that overlapped with bins 23:32 of the LISST [*Mikkelsen et al.*, 2004].

[20] The LISST and DFC particle size distributions overlapped across 10 bins (bins 23:32) with nominal diameters from 47.7 to 250 μm. In this overlap region, volume concentrations from the DFC and LISST instruments did not agree precisely (Figure 3). In particular, it was common for LISST concentrations to decrease in the upper end of the overlap bins where concentrations measured by the DFC increased. A possible explanation for this divergence is that the LISST recognizes component particles within flocs as independent, whereas the DFC images them as part of the whole. To contend with this uncertainty, a new method was developed for combining data from the LISST and DFC (Figure 3). On a sample-by-sample basis, an overlap size bin was selected as the "merge bin" at which the two size distributions were joined. Bins less than or equal to the merge

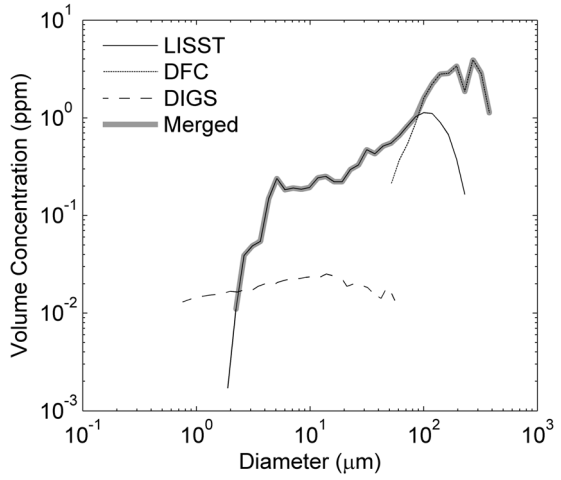

Figure 3. Example of a combined size distribution (solid gray line) generated by merging LISST (solid black line) and DFC (dotted line) data, accompanied by the associated disaggregated inorganic grain size (DIGS) distribution (dashed line) measured from filters of the suspension collected in situ and at the same time. The merge bin between LISST and DFC distributions is chosen by comparing the projected area of the combined distribution to the beam attenuation coefficient. The merge bin that gives a total projected particle area closest to twice the attenuation coefficient is selected. Note that the LISST concentrations decrease at the upper end of the measured range, while the DFC concentrations increase over the same range. This effect likely arises because the LISST interprets the components of large flocs as independent entities, while the DFC recognizes the components as parts of a larger aggregate. The DIGS distribution suggests that the smallest particles in suspension are contained within larger aggregates, supporting the assumption (see text) that particles small with respect to the wavelength of light do not contribute significantly to attenuation.

bin were assigned concentrations from the LISST. Bins greater than the merge bin were assigned concentrations from the DFC. The merge bin was selected to minimize the difference between the beam attenuation measured by the LISST and two times the total particle area concentration of the resultant merged spectrum.

[21] The strategy for merging data from the LISST and DFC assumes that the majority of particles were much larger than the wavelength of light, so they had attenuation efficiencies equal to 2. It also assumes that the acceptance angle of the LISST is small enough to recognize light scattered from large particles in the very near forward as scattered rather than transmitted. The merged distributions were truncated on the lower end at a size of 2.05 μm. On the upper end, the distributions were truncated at the largest size bin below which all concentrations were nonzero. Implicit in this treatment of the size distribution are the assumptions that particles smaller than 2.05 μm and large, rare particles do not contribute significantly to optical attenuation in the bottom boundary layer. This first assumption is at odds with other studies that argue that small particles contribute significantly to attenuation [e.g., *Babin et al.*, 2003], but it receives support from the LISST size distributions, which show steep decreases in particle concentrations below diameters of approximately 5 μm (Figure 3). Our in situ observations of undisturbed particle size distributions indicate that the smallest particles in suspension likely are contained within aggregates. Supporting this hypothesis are the disaggregated particle size distributions measured from filters that show that particles smaller than 5 μm are present but not as individual entities.

[22] The LISST and DFC together measured size distribution and c_p at 5-min intervals during extended deployments. It was not possible to gather direct observations of *SPM* at the same temporal resolution or over the same range of conditions. Therefore *SPM* was estimated from measured volume distributions by multiplying the volume concentration in each size bin by the density of a sphere with the nominal diameter of the size bin [*Curran et al.*, 2007]. Nominal densities were estimated by fitting a model [*Khelifa and Hill*, 2006] to in situ size-versus-settling-velocity data.

[23] The settling column equipped with a digital video camera was used to measure particle size and settling velocity. The column was equipped with a baffled top and a lid that rotated onto the top of the column 15 s prior to the measurement period. These features minimized flow disruptions of settling particles within the column. As particles settled in the column, 1-min video clips were recorded to 80-min mini Digital Video (miniDV) tapes. The 80, 1-min video clips were spread equally throughout each deployment period. For each clip, a sequence of four frames was used to estimate the mean equivalent circular diameter, settling distance, and settling time (the elapsed time of the four images) for each particle that appeared in at least 3 of the frames [*Fox et al.*, 2004]. Floc effective density ($\rho_a - \rho$), where ρ_a is the floc bulk density (g m^{-3}) and ρ is the density of seawater (g m^{-3}), was estimated for each particle based on its settling velocity and diameter [*Khelifa and Hill*, 2006]. The model is based on analysis of 26 published data sets and designed to be a general tool for describing settling velocity and density as function of aggregate size. It accounts for decreasing floc density with increasing floc size in a way that is consistent with observations from the literature. In the model, $\rho_a - \rho$ follows the form

$$\rho_a - \rho = (\rho_s - \rho)\left(\frac{D}{D_c}\right)^{F-3}, \tag{9}$$

where ρ_s is the density of the component grains in the flocs, D is the floc diameter, D_c is the median component grain size diameter, and F relates particle mass to particle diameter. It is akin to a size-specific fractal dimension. The term F is given by

$$F = \alpha\left(\frac{D}{D_c}\right)^{\beta}, \tag{10}$$

where α and β are coefficients that relate F to particle size. The parameter α is equal to 3. This value forces the fractal dimension to 3 as aggregate diameter approaches the diameter of the component particles. The value of β is given by the equation

$$\beta = \frac{\log\left(\frac{F_{\max}}{3}\right)}{\log\left(\frac{D_{\max}}{D_c}\right)}. \tag{11}$$

In equation (11), F_{max} is the value of F for the largest flocs, and D_{max} is the diameter of the largest flocs. Settling velocities were fit to particle diameters according to this equation:

$$w_s = \frac{g(\rho_s - \rho)}{18\mu} D_c^{3-F} \frac{D^{F-1}}{1 + 0.15\mathrm{Re}^{0.687}}, \quad (12)$$

where w_s is the particle settling velocity, g is the gravitational acceleration, μ is the dynamic viscosity of seawater, and Re is the particle Reynolds number [*Khelifa and Hill*, 2006]. Component particle diameter (D_c) was taken as the volumetric median diameter of the disaggregated inorganic suspended particle size distribution captured by the in situ filtration system. The variable D_{max} was computed from the 95th percentile of the floc diameters from the digital video camera on the settling column. Outlier diameters were not included. Outliers were identified by first binning the data into diameter bins, then discarding those particles with diameters not within 2 standard deviations of the bin median. The density and viscosity of water were calculated from temperature and salinity measured at MVCO. Values of F_{max} and ρ_s were found using a least squares fit of the model to the data. Mass concentration in each bin was estimated by multiplying volume concentration in each bin by the bin-specific particle densities estimated from equations (9)–(12). *SPM* was calculated by summing the mass concentrations in each bin. In this way, *SPM* was estimated over the same range of conditions and temporal resolution as c_p and particle size.

[24] Accuracy of estimated *SPMs* was gauged by comparison with *SPM* measured from filtered samples. These samples were collected with the McLane water transfer system, which filtered a specified volume of a suspension through one of 24 filters. The intake for the transfer system was located at the same height as the other instruments, and the 24 samples were spaced equally throughout each deployment. Preweighed Millipore 8.0-μm SCWP (cellulose acetate) filters were used in the water transfer system. These filters were selected because they have effective pore sizes that are much lower than the nominal size, and they combine excellent trapping efficiency while minimizing clogging [*Sheldon*, 1972]. The filters were rinsed with super Q water to remove salts, then dried at 60°C and weighed to determine SPM concentration. For analysis of the size distribution of disaggregated grains in suspension, the filters were placed in a low-temperature (60°C) oxygen/plasma asher to remove the filter and organic matter while preventing the fusing of mineral grains. The remaining inorganic suspended sediments were resuspended in a 1% NaCl electrolytic solution before disaggregation with a sapphire-tipped ultrasonic probe. Size distributions were measured with a Coulter Multisizer IIe [cf. *Law et al.*, 2008], and geometric mean diameter was calculated.

[25] To estimate stress in the bottom boundary layer, an iron beam equipped with acoustic Doppler velocimeters (ADVs) was deployed. The ADVs were spaced alongshore at x = 0.0, 1.0, and 3.0 m. All sensors were 0.75 m above bottom. The sample rate was 20 Hz, and the measurements were processed in hour-long bursts. A direct estimation of the hour-averaged Reynolds stress was calculated following procedures outlined by *Trowbridge and Elgar* [2003]. To estimate the oscillatory wave-current stress at the seafloor, the Grant-Madsen model [*Grant and Madsen*, 1986] was applied, with a fixed value of the physical hydrodynamic roughness z_o. The model inputs were the ADV-derived mean velocity, standard deviation of the wave-induced oscillatory velocity, dominant wave period, and angle between the mean and wave-induced oscillatory velocity. The model outputs are the shear velocity associated with the mean stress, the shear velocity associated with the maximum wave and current stress at the seafloor, and the shear velocity associated with the maximum wave stress at the seafloor. Shear velocities reported here (Figures 2 and 4) are associated with the maximum wave and current stress at the seafloor. The global value of z_o was estimated by determining the best fit of the measured and modeled stresses.

4. Results

[26] Weather at MVCO in September 2007 forced a range of values in particle size and in the beam attenuation coefficient (Figure 4). Median particle size from merged spectra ranged from less than 10 μm up to 150 μm, and the beam attenuation ranged from approximately 1 to 15 m^{-1}. Large particle sizes and beam attenuation coefficients were associated with three resuspension events in the middle of the month that were forced by strong winds and large waves from the south (Figures 2 and 4). During these events, peaks in combined wave and current seabed stress led peaks in median particle diameter and c_p. This pattern is associated with sediment limitation in the seabed [*Wiberg et al.*, 1994]. In short, as stress builds, sediment fine enough to be resuspended is mixed into a bottom boundary layer that is thick because of the high stress. High stress limits aggregate size, and a thick boundary layer combined with limited sediment availability causes lower values of c_p. As the stress wanes due to decreasing winds and waves, large aggregates form because of lowered stresses and elevated sediment concentration [*Manning et al.*, 2006; *Mikkelsen et al.*, 2006; *Milligan et al.*, 2007; *Xu et al.*, 2008]. The beam attenuation coefficient rises as sediment remains suspended but in a thinner boundary layer. Eventually, median particle diameter and c_p decrease to low values because of sedimentation at low stress [*Manning et al.*, 2006; *Mikkelsen et al.*, 2006; *Xu et al.*, 2008].

[27] Size-settling velocity data were used to estimate two parameters for the *Khelifa and Hill* [2006] model of aggregate density: F_{max}, which is the "fractal dimension" of the largest aggregates in suspension, and ρ_s, which is the density of the component grains. Because of large scatter due to variable particle composition, these parameters cannot be estimated precisely from a single video clip, so estimates were made by pooling data from many clips. The clips were grouped by deployment and by seabed stress. Neither of these groupings produced significantly different values of F_{max} or ρ_s among deployments, implying that, despite significant variability of particles within the population, all particles in the five deployments can be considered to have come from the same population [*Ganju et al.*, 2006] (Tables 1 and 2). This postulate is consistent with the hypothesis that local resuspension supplies sediment to the bottom boundary layer. Because of the lack of discernible differences among groups, all size-settling velocity data were merged, and the *Khelifa and Hill* [2006] model was fit to the entire data set. Resulting values for F_{max} and ρ_s were 2.25 and 1.150 g m^{-3}, respectively. The low density of aggregates indicates that they

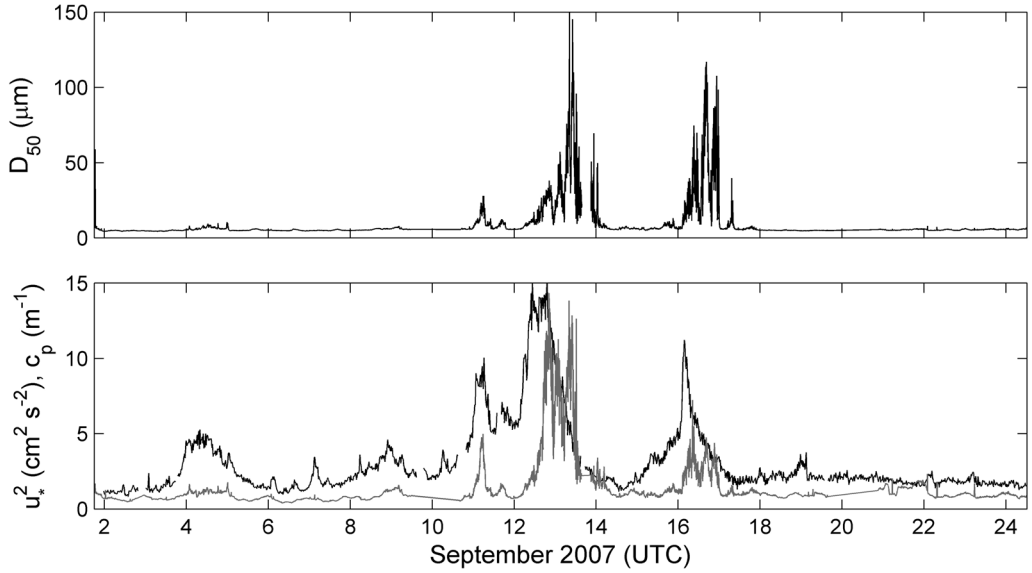

Figure 4. (top) Median diameter (D50) and (bottom) beam attenuation coefficient (gray line) and the square of the wave plus current shear velocity (black line) at the 12-m node of MVCO plotted versus date. Median diameter and the beam attenuation increase when stress increases, but with some lag. The covariation of stress, size, and beam attenuation coefficient likely indicates that local resuspension is the source of suspended particles. The lag is likely due to sediment limitation in the seabed. See text for details. Note the order-of-magnitude ranges in beam attenuation coefficient and median diameter during the experiment. This range allows examination of the effect of particle size on c_p:*SPM* over a broad range of conditions.

were organic rich. The value of the fractal dimension of the largest aggregates is similar to values measured in other studies [*Syvitski et al.*, 1995; *Hill et al.*, 1998; *Sternberg et al.*, 1999; *Fox et al.*, 2004].

[28] Measured *SPM* and *SPM* estimated with the above inputs are linearly related, but the slope of a best fit linear regression of estimated *SPM* on measured *SPM* equals 1.83 and is significantly greater than unity (Figure 5). This result indicates that the method for estimating SPM from volume distributions overpredicts the suspended particulate mass concentration. Other studies comparing measured *SPM* and *SPM* estimated from size distributions have found similar results [*Curran et al.*, 2002, 2004; *Fox et al.*, 2004]. A reasonable explanation for overestimation of *SPM* is application of an incorrect drag law that does not account for drag reduction caused by passage of fluid through large throats in loose particle aggregates [*Li and Logan*, 1997]. Reduction of drag means that a fractal, porous and permeable aggregate will sink faster than an equal-sized solid sphere of the same mass. Failure to account for this effect results in overestimation of particle mass and density, and as a result, suspended particulate mass. This explanation receives some support from examination of the relationship of estimated to measured *SPM* at lower values (Figure 5). Nearer the origin, the slope of the best fit of estimated to measured *SPM* is closer to 1. Particles at low concentrations were smaller (Figure 4) and likely had fractal dimensions closer to 3, so errors arising from failure to account for the fractal geometry of flocs should be less. Another possibility for mismatch between estimated and measured *SPM* is that the settling model for the smallest particles in the distribution is in error because direct observations of the size-settling velocity relationship only extend to particles as small as approximately 100 μm diameter. A third possibility for overestimation of SPM is bias in the measured SPM arising from use of filters with a large nominal pore size that allow a significant fraction of the suspended mass smaller than the nominal pore size to pass through the filter. This explanation is unlikely because the Millipore 8.0-μm SCWP (cellulose acetate) filters used in this study have high trapping efficiencies and because the effective filtration diameter is much below the nominal pore size [*Sheldon*, 1972; Figure 3].

[29] Accounting for any of these causes of mismatch between measured and estimated SPM is not possible with the data that were collected, so estimated SPM were corrected

Table 1. Floc Geometry Parameters for Each Deployment

Deployment	D_c (μm)	D_{max} (μm)	ρ_s(g m^{-3})	F_{max}
1–2 Sep	4.4	1055	1.295	2.2
2–9 Sep	4.3	942	1.170	2.3
10–13 Sep	8.8	454	1.125	2.3
13–19 Sep	6.6	1073	1.130	2.2
20–24 Sep	4.2	1014	1.220	2.2
Mean	5.7	908	1.188	2.2

Table 2. Floc Geometry Parameters for Five Equal Shear Velocity Ranges

u_* Range (m s^{-1})	D_c (μm)	D_{max} (μm)	ρ_s(g m^{-3})	F_{max}
0.009–0.015	4.6	1075	1.130	2.3
0.015–0.021	5.4	984	1.170	2.2
0.021–0.026	8.2	886	1.100	2.3
0.026–0.032	8.6	429	1.225	2.1
0.032–0.038	9.5	588	1.120	2.3
Mean	7.3	792	1.149	2.2

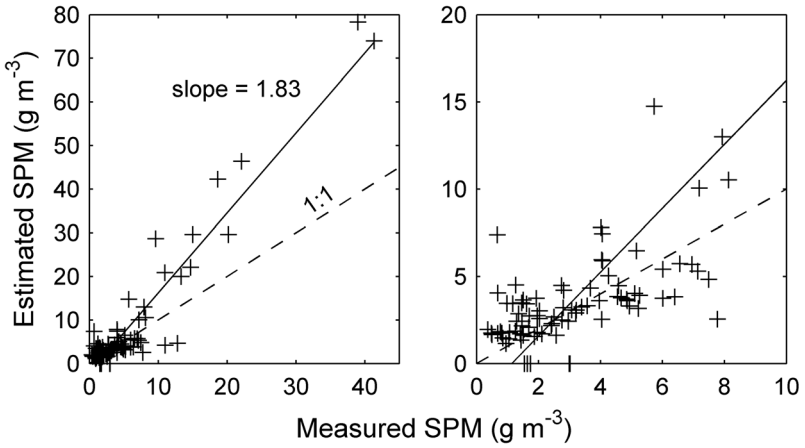

Figure 5. Estimated *SPM* plotted versus *SPM* measured with the in situ filtration system, showing (left) data over the entire range of measured and estimated values. A best fit linear regression ($r^2 = 0.89$, N = 96) yields a slope of 1.83 (solid line), indicating that estimated *SPM* are overestimates. The slope of this line is significantly different from the dashed line with a 1:1 slope ($p < 0.001$). The most likely source of error is application of an incorrect drag law to porous and permeable flocs (see text for details). If an incorrect drag law is the source of error in estimated SPM, then the magnitude of error should be smaller for smaller particles because they are less porous and permeable than the larger, looser flocs. Also shown is (right) the comparison of estimated to measured *SPM* when concentrations and particle sizes were smaller. The slope of a line fit to these data (solid line) is closer to the 1:1 (dashed) line, supporting the hypothesis that an incorrect drag law leads to overestimation of the mass of flocs.

empirically. Under the assumption that an incorrect drag law was the source of error in estimation of *SPM*, a drag correction factor was determined iteratively. For a range of drag correction factors, the Khelifa-Hill model was used, with the drag reduced, to estimate corrected *SPM*, as described in section 3. The sum of the squares of the differences between the estimated and measured masses was then computed for each drag correction factor. The correction factor that yielded the smallest sum of squared differences was determined. The resulting drag correction factor was 0.58. This correction brings estimated SPM into the range of measured SPM (Figure 6).

[30] The relationship between c_p and *SPM* is linear, with a slope plus or minus two standard deviations of 0.22 ± 0.0015 g m^{-2} (Figure 6). The value of this slope, which is

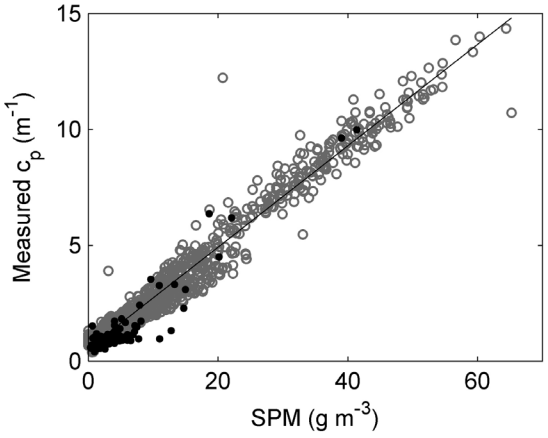

Figure 6. Beam attenuation coefficient (c_p) plotted versus suspended particulate mass (*SPM*). Closed black circles are associated with values of *SPM* measured with the in situ filtration system. Open gray circles are values associated with *SPM* estimated every 5 min from the merged size spectra and the size-settling velocity data. To bring the data cloud of estimated SPM into line with measured SPM, a drag correction factor of 0.58 was applied to the conversion of settling velocity to floc density. The linearity of the relationship between c_p and *SPM* over a broad range of values indicates c_p*:SPM* does not vary widely during the course of the experiment. The slope of the relationship plus or minus two standard deviations is 0.22 ± 0.0015 m^2 g^{-1}.

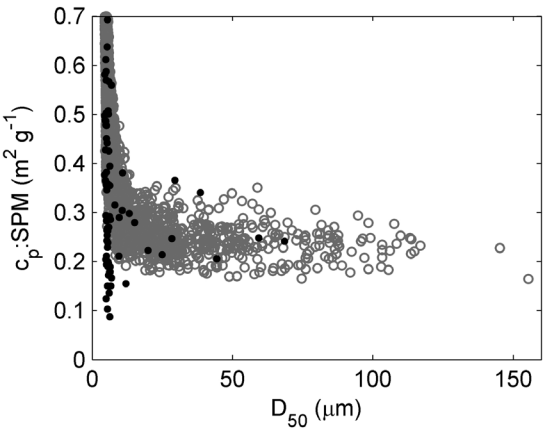

Figure 7. The ratio c_p*:SPM* plotted versus median particle size. Closed black circles are associated with values of *SPM* measured with the in situ filtration system. Open gray circles are values associated with *SPM* estimated every 5 min from the merged size spectra and the size-settling velocity data. When median particle size is small, c_p*:SPM* is variable, but when median particle size grows larger than 10 μm, the value of c_p*:SPM* is constrained between 0.2 and 0.4 m^2 g^{-1}.

equal to c_p:*SPM*, is in the general range of 0.2–0.6 g m^{-2} found in the recent study by *Boss et al.* [2009c], although it is important to note that the acceptance angle of the SeaTech transmissometers used in the Boss study is significantly larger than the acceptance angle of this LISST. Linearity applies over a large range of *SPM* and c_p despite large variability in particle size. When c_p:*SPM* is plotted versus median diameter, it is apparent that over a large size range, this ratio is relatively constant, varying only over a factor of about 2 (Figure 7). When median diameters are small, however, c_p:*SPM* values range over a factor of 10 (Figure 7). These results indicate that variable particle size is not the primary factor in generating variability in c_p:*SPM*, and they are consistent with theoretical and field work that place predicted values in the range of 0.2–0.6 [*Boss et al.*, 2009b, 2009c]. Other factors must be responsible the wide range of literature values of c_p:*SPM*.

5. Discussion

[31] The results show that particle size does not affect c_p:*SPM* as strongly as predicted by theory for solid particles. Over a range in median particle size from 10 to over 100 μm, c_p:*SPM* is constrained to values between 0.2 and 0.4. This factor-of-two range is much smaller than the more than factor-of-ten range that would obtain if the particles were solid. This relative insensitivity of c_p:*SPM* to particle size supports the theoretical work of *Boss et al.* [2009b] that attributes lack of sensitivity to size to the fractal geometry of natural particles. The results support the application of transmissometers to estimation of suspended particulate mass in coastal waters, even in the presence of widely varying particle size. That said, the need for careful calibration to obtain the appropriate c_p:*SPM* remains because this ratio is observed to vary by over an order of magnitude across different environments (Figure 1). Lack of sensitivity of c_p:*SPM* to particle size measured here indicates that the range in literature values arises from another source. Possible causes of variability are systematic measurement bias, particle composition, and particle packing geometry.

[32] One source of systematic measurement bias stems from a finite acceptance angle for measurement of light transmission [*Piskozub et al.*, 2004; *Boss et al.*, 2009a]. Optical instruments accept a small range of angles on either side of a directly transmitted beam as transmitted rather than scattered in the near forward direction. *Piskozub et al.* [2004] and M. Jonasz and E. Boss (see http://www.tpdsci.com/Tpc/VsfSmlAngNatDsp.php) argue that the amount of scattered light that is recorded as transmitted could be large, accounting for as much as 50–80% of the total scattering for large scatterers like bubbles. More importantly, the magnitude of this forward scattering error depends on particle size, because small particles tend to scatter light more isotropically than large particles, which scatter strongly in the near-forward [*Piskozub et al.*, 2004; *Boss et al.*, 2009a]. As particles in a suspension clump to form large aggregates, it is possible that a growing fraction of the scattered light would be recognized by the sensor as transmitted light, thereby driving the c_p:*SPM* toward lower values. Because more concentrated suspensions often are more aggregated [e.g., *Milligan et al.*, 2007], c_p:*SPM* values may fall with increasing sediment concentration. *Boss et al.* [2009a] provided evidence of this effect by codeploying transmissometers with different acceptance angles. When the particle size distribution was relatively enriched in large particles, the difference in the beam attenuation coefficient measured by a SeaTech transmissometer, with a relatively large acceptance angle, was less than half the attenuation coefficient measured by a Sequoia Scientific LISST 100x Type Floc, with a relatively small acceptance angle. When large particles were rarer, the beam attenuation coefficients measured by the two instruments converged.

[33] The majority of estimates of c_p:*SPM* in Figure 1 were collected with SeaTech 25-cm-path length transmissometers, which have an acceptance angle just over 1°. If a substantial fraction of the total mass in suspension resided in particles with diameters larger than about 10 μm, then attenuation could be underestimated by a factor of about 2 for weakly absorbing particles [*Boss et al.*, 2009a], explaining a significant portion of the variability in literature values of c_p:*SPM*. If this proposed indirect effect of particle size on c_p:*SPM* does explain covariation between c_p:*SPM* and suspended sediment concentration, then the effect would be less significant in this study because the LISST 100x Type B has an acceptance angle of only 0.026°. With such a small acceptance angle, only when aggregates grow to over 100 μm should an effect be noticeable, and then observed attenuation coefficients theoretically would be reduced by less than 25% [*Boss et al.*, 2009a]. It is interesting to note, however, that the value of c_p:*SPM* measured in this study with an instrument with a small acceptance angle falls in the range of literature values measured at similar maximum concentrations with instruments with a larger acceptance angle. If acceptance angle was the primary source of variability in c_p:*SPM*, then values estimated with instruments with small acceptance angles like the LISST 100x should yield higher estimates of c_p:*SPM* than those yielded by instruments with larger acceptance angles. Overall, use of instruments with smaller acceptance angles will reduce the potential bias and/or unconstrained variability in c_p:*SPM* introduced by forward scattering error [*Piskozub et al.*, 2004], but unfortunately smaller acceptance angles also reduce the signal-to-noise ratio.

[34] Multiple scattering is another potential source of measurement bias that could cause c_p:*SPM* to fall with increasing concentration. The linear correlation between c_p and *SPM* (equation (5)) is based on the assumption that photons scattered by a particle are permanently lost from the transmitted beam. Some photons that are scattered away from the receiver by a particle, however, can be scattered back toward the receiver by subsequent scattering by another particle. In this way, multiple scattering can increase transmission of light to the receiver, thereby reducing the measured beam attenuation coefficient [*Piskozub et al.*, 2004] and values of c_p:*SPM*. Multiple scattering becomes a factor when the optical depth, which is the product of path length and beam attenuation coefficient, exceeds 0.3 [*van de Hulst*, 1981; *Piskozub et al.*, 2004]. This limit, of course, is dependent on the angular distribution of scattered light, and it will be larger for suspensions richer in large particles. Nonetheless, for a 25-cm path length transmissometer, as used in most of the studies in Figure 1, c_p values above 1.2 will be affected by multiscattering error. At such low values, maximal c_p:*SPM* values are near unity (Figure 1), indicating that multiple scattering affects most of the measurements in the literature.

Theoretical work, however, shows that the error is not large as long as optical depths remain below 10. For suspensions of small particles, maximum underestimation of c_p would be 28%, whereas for large particles underestimation would be only a few percent [*Piskozub et al.*, 2004], which interestingly shows that multiple scattering at high concentrations acts to reduce the effect of particle size on estimates of c_p*:SPM*.

[35] To determine approximately what sediment concentration is associated with an optical depth of 10, consider a 25-cm path length transmissometer and an assumed c_p*:SPM* of 0.5, which is the approximate median of the literature values in Figure 1. With these parameters an optical depth of 10 corresponds to a sediment concentration of 80 g m^{-3}. For the LISST 100x Type B used in this study, which has a 5-cm path length, and a c_p*:SPM* of 0.22, the sediment concentration associated with an optical depth of 10 is slightly greater than 900 g m^{-3}. Only two of the literature values for c_p*:SPM* derive from environments where maximal sediment concentration was greater than or equal to 80 g m^{-3}, suggesting that multiple-scattering error is small.

[36] Particle composition can also contribute to variability in c_p*:SPM*. *Babin et al.* [2003] conducted a theoretical evaluation of the effect of particle composition on scattering, and because attenuation at the wavelengths used by most transmissometers is dominated by scattering, the results of their analysis are applicable here. In short, they found that a change from organic matter to inorganic matter can reduce c_p*:SPM* by a factor of 2. They argued that composition can explain the reduction in c_p*:SPM* moving from deep water, where particles tend to be biogenic, to shallow water, where mineral particles are more common because of input from land and resuspension from the seabed. The reason for the reduction is the density difference between organic and inorganic particles. Bulk density of organic matter is near that of water, while densities of typical inorganic minerals range from 1.9 to 2.8 g m^{-3}. As a result, the areal cross section per unit mass for an organic particle typically is more than twice as large as for an inorganic particle of the same size. Organic particles, however, have a lower refractive index than inorganic particles, which reduces the effect of composition to the factor of 2 proposed by *Babin et al.* [2003]. Because the higher values of sediment concentration in Figure 1 come from coastal environments where inorganic particles in suspension would be more common, the fall in c_p*:SPM* with increasing concentration may be explained in part by a shift in particle composition. Recent field observations by *Bowers et al.* [2009] support this explanation for variability in mass-normalized scattering coefficients. They conclude that 65% of the variability in the ratio of scattering coefficient to *SPM* is due to particle density, and only 15% of the variability is due to particle size.

[37] A final explanation for the observed decrease in c_p*:SPM* with increasing sediment concentration is variable particle packing geometry, as embodied in the fractal dimension F (equation (10)). Observations in a range of environments show that F can vary widely, from just over 1 to just under 3. Values tend to cluster around 2, however, with 1.8 as a representative lower bound and 2.4 as a representative upper bound [*Logan and Wilkinson*, 1990; *Syvitski et al.*, 1995; *Hill et al.*, 1998; *Dyer and Manning*, 1999; *Fox et al.*, 2004]. Theoretically, sticky particles form loose aggregates with lower fractal dimensions than less sticky particles. The basis for this argument is that less sticky particles can adjust position within an aggregate, and in the process become closer to neighboring particles. Particle adjustments produce denser aggregates, explaining why sticky organic aggregates often have lower fractal dimensions than less sticky inorganic aggregates [*Logan and Wilkinson*, 1990]. Fractal dimension can affect c_p*:SPM* by affecting particle density as a function of size. For two aggregates with the same geometric cross section and made up of the same size component grains, the one with the larger fractal dimension will be denser (equation (9)). As a result, its cross-sectional area per unit mass will be smaller, driving down the c_p*:SPM* ratio in the suspension.

[38] The effect of particle packing geometry on c_p*:SPM* likely is small. In the extreme, a fractal dimension of 3 would produce a particle with a density equal to its component particles, while a fractal dimension much less than 2 would produce an aggregate with a density near that of water. This extreme situation would produce variability in c_p*:SPM* similar to the variability caused by organic versus inorganic particle composition. Realistically, the effect of particle packing geometry would be much less. Consider a situation in which aggregates are 50 times larger in diameter than their component grains, e.g., 250-μm diameter aggregates formed from 5-μm diameter component particles. Assuming a component particle density of 1.15 g m^{-3} estimated here, a seawater density of 1.025 g m^{-3}, and a range of fractal dimensions from 1.8 to 2.4, equation (9) indicates that floc density changes by approximately 1%.

[39] This analysis of sources of variability in c_p*:SPM* identifies particle composition as an important parameter in the conversion of an optical signal into suspended particulate mass. Caution is necessary, therefore, in interpretation of optical data gathered from environments where composition varies widely. Variability is evident in this data set when median particle sizes were small (Figure 7), which occurred when stresses were small, resuspension was absent, and biological processes plus advection of coastal water masses determined the composition of particles in suspension. Local resuspension events homogenized the particle composition and reduced the variability in c_p*:SPM*. In the presence of compositional variability, a few options exist for constraining the value of c_p*:SPM*. The first is to employ traditional calibrations with directly measured *SPM* throughout a time series. This strategy is usually not practical. A pragmatic solution is to use the trend in Figure 1 to constrain c_p*:SPM* based on maximum observed sediment concentration. A third option is to measure optical properties that can serve as a proxy for composition. *Boss et al.* [2009c] and *Loisel et al.* [2007] showed that the backscattering-to-beam-attenuation ratio and the ratio of POC to SPM are inversely correlated. On the basis of such measurements, different values for c_p*:SPM* could be assigned to different periods in a deployment, thus improving the accuracy of the conversion from beam attenuation to suspended particulate mass.

6. Conclusions

[40] A large fraction of the suspended particulate mass of marine particles is contained in aggregates that incorporate increasingly large void fractions as they grow in size. As a result, solid mass within aggregates scales more closely with

particle projected area than with particle volume. Because optical attenuation due to large particles also scales with projected area, c_p and *SPM* retain a linear correlation even when particle size varies. The theoretical basis for this hypothesis [*Boss et al.*, 2009b] now has firm support from the field measurements reported here.

[41] For years, the order-of-magnitude variability in the ratio of c_p to *SPM* has been attributed to variable particle size, but results here suggest that variability due to particle size only accounts for a factor-of-two range in c_p:*SPM*. Another factor-of-two range in the value of c_p:*SPM* likely arises from compositional variability of suspended particles. Organic particles with densities near that of water have higher projected area per unit of solid mass than inorganic particles that have densities 2 to 3 times larger. The effect of the density difference is muted by the lower refractive index of watery organic particles. Another possible source of factor-of-two variability is due to the effect of finite instrument acceptance angles, especially with the commonly used SeaTech 25-cm path length transmissometer. For large particle aggregates, these devices may recognize light scattered in the near forward direction as transmitted light, lowering the beam attenuation coefficient and c_p:*SPM*. Because large aggregates are more abundant when *SPM* is large, forward scattering error should also grow with increasing sediment concentration. Multiple scattering error and aggregate packing geometry likely do not affect c_p:*SPM* significantly. Together, variable composition, size, and forward scattering error can explain the order-of-magnitude variability in literature values of c_p:*SPM*.

[42] The constrained response of transmissometers, and by implication other optical sensors, to particle size explains why such devices, with adequate calibration, have provided reasonably accurate estimates of suspended particulate mass in natural waters. Accuracy in the conversion from an optical property to *SPM* would benefit from the development and implementation of simple optical proxies of particle composition. Forward scattering error is reduced significantly by use of transmissometers with small acceptance angles. With these improvements to technology, transmissometers can provide accurate estimates of suspended particulate mass even in the presence of widely varying particle sizes.

Notation

c_p beam attenuation coefficient, m^{-1}.
c_p:*SPM* mass normalized beam attenuation coefficient, $m^2\ g^{-1}$.
D particle diameter, μm.
D_c component particle diameter in aggregates, μm.
D_{max} maximal particle diameter, μm.
D_{min} minimal particle diameter, μm.
f_m mass frequency distribution, m^{-1}.
F aggregate fractal dimension, dimensionless.
F_{max} fractal dimension of largest aggregates, dimensionless.
g gravitational acceleration, $m\ s^{-2}$.
H_s significant wave height, m.
J intensity of transmitted light, cd.
J_o intensity of transmitted light in particle-free water, cd.
L transmissometer path length, m.
$m(D)$ suspended particulate mass concentration density function, $g\ m^{-4}$.
$n(D)$ suspended particulate number concentration density function, m^{-4}.
$Q_c(D)$ attenuation efficiency, dimensionless.
Re particle settling Reynolds number, dimensionless.
SPM suspended particulate mass concentration, $g\ m^{-3}$.
T_p dominant wave period, s.
u_* wave plus current shear velocity, $m\ s^{-1}$.
w_s particle settling velocity, $m\ s^{-1}$.
α particle geometry parameter, dimensionless.
β particle geometry parameter, dimensionless.
μ fluid dynamic viscosity, $g\ m^{-1}\ s^{-1}$.
ρ_a aggregate density, $g\ m^{-3}$.
ρ_s component particle density, $g\ m^{-3}$.
ρ fluid density, $g\ m^{-3}$.

[43] **Acknowledgments.** This work was supported by the United States Office of Naval Research. We thank John Trowbridge from Woods Hole Oceanographic Institution for providing stress data, and we gratefully acknowledge the support of the Captains and crews of the R/V *Tioga* and R/V *Connecticut*. Janet Fredericks, Jay Sisson, and the WHOI divers provided valuable technical assistance, as did Wayne Slade and Jim Loftin from the University of Maine. Finally, we wish to thank Kristian Curran, formerly of Dalhousie University and now with Fisheries and Ocean Canada, for his work and support during the project.

References

Agrawal, Y. C., and H. C. Pottsmith (2000), Instruments for particle size and settling velocity observations in sediment transport, *Mar. Geol.*, *168*(1–4), 89–114, doi:10.1016/S0025-3227(00)00044-X.

Babin, M., A. Morel, V. Fournier-Sicre, F. Fell, and D. Stramski (2003), Light scattering properties of marine particles in coastal and open ocean waters as related to the particle mass concentration, *Limnol. Oceanogr.*, *48*(2), 843–859, doi:10.4319/lo.2003.48.2.0843.

Baker, E. T., and J. W. Lavelle (1984), The effect of particle size on the light attenuation coefficient of natural suspensions, *J. Geophys. Res.*, *89*(C5), 8197–8203, doi:10.1029/JC089iC05p08197.

Berry, M. V., and I. C. Percival (1986), Optics of fractal clusters such as smoke, *J. Mod. Opt.*, *33*(5), 577–591, doi:10.1080/713821987.

Bishop, J. K. B. (1999), Transmissometer measurement of POC, *Deep Sea Res., Part I*, *46*(2), 353–369, doi:10.1016/S0967-0637(98)00069-7.

Boss, E., W. H. Slade, M. Behrenfeld, and G. Dall'Olmo (2009a), Acceptance angle effects on the beam attenuation in the ocean, *Opt. Express*, *17*(3), 1535–1550, doi:10.1364/OE.17.001535.

Boss, E., W. Slade, and P. Hill (2009b), Effect of particulate aggregation in aquatic environments on the beam attenuation and its utility as a proxy for particulate mass, *Opt. Express*, *17*(11), 9408–9420, doi:10.1364/OE.17.009408.

Boss, E., et al. (2009c), Comparison of inherent optical properties as a surrogate for particulate matter concentration in coastal waters, *Limnol. Oceanogr. Methods*, *7*, 803–810.

Bowers, D. G., K. M. Braithwaite, W. A. M. Nimmo-Smith, and G. W. Graham (2009), Light scattering by particles suspended in the sea: The role of particle size and density, *Cont. Shelf Res.*, *29*(14), 1748–1755, doi:10.1016/j.csr.2009.06.004.

Bricaud, A., A. Morel, and L. Prieur (1981), Absorption by dissolved organic matter of the sea (yellow substance) in the UV and visible domains, *Limnol. Oceanogr.*, *26*(1), 43–53, doi:10.4319/lo.1981.26.1.0043.

Bunt, J. A. C., P. Larcombe, and C. F. Jago (1999), Quantifying the response of optical backscatter devices and transmissometers to variations in suspended particulate matter, *Cont. Shelf Res.*, *19*(9), 1199–1220, doi:10.1016/S0278-4343(99)00018-7.

Curran, K. J., P. S. Hill, and T. G. Milligan (2002), Fine-grained suspended sediment dynamics in the Eel River flood plume, *Cont. Shelf Res.*, *22*(17), 2537–2550, doi:10.1016/S0278-4343(02)00129-2.

Curran, K. J., P. S. Hill, T. G. Milligan, E. A. Cowan, J. P. M. Syvitski, and S. M. Konings (2004), Fine-grained sediment flocculation below the Hubbard Glacier meltwater plume, Disenchantment Bay, Alaska, *Mar. Geol.*, *203*(1–2), 83–94, doi:10.1016/S0025-3227(03)00327-X.

Curran, K. J., P. S. Hill, T. G. Milligan, O. A. Mikkelsen, B. A. Law, X. Durrieu de Madron, and F. Bourrin (2007), Settling velocity, effective density, and mass composition of suspended sediment in a coastal bottom

boundary layer, Gulf of Lions, France, *Cont. Shelf Res.*, *27*(10–11), 1408–1421, doi:10.1016/j.csr.2007.01.014.

Downing, J. (2006), Twenty-five years with OBS sensors: The good, the bad, and the ugly, *Cont. Shelf Res.*, *26*(17–18), 2299–2318, doi:10.1016/j.csr.2006.07.018.

Dyer, K. R., and A. J. Manning (1999), Observation of the size, settling velocity and effective density of flocs, and their fractal dimensions, *J. Sea Res.*, *41*(1–2), 87–95, doi:10.1016/S1385-1101(98)00036-7.

Edson, J., T. Austin, W. McGillis, M. Purcell, R. Petitt, J. Ware, M. McElroy, S. Hurst, and C. Grant (2001), The Martha's Vineyard Coastal Observatory, paper presented at OHP/ION Joint Symposium on Long-term Observations in the Oceans, Int. Ocean Network, Mt. Fuji, Japan.

Fabricius, K. E., and E. Wolanski (2000), Rapid smothering of coral reef organisms by muddy marine snow, *Estuarine Coastal Shelf Sci.*, *50*(1), 115–120, doi:10.1006/ecss.1999.0538.

Fox, J. M., P. S. Hill, T. G. Milligan, A. S. Ogston, and A. Boldrin (2004), Floc fraction in the waters of the Po River prodelta, *Cont. Shelf Res.*, *24*(15), 1699–1715, doi:10.1016/j.csr.2004.05.009.

Fugate, D. C., and C. T. Friedrichs (2002), Determining concentration and fall velocity of estuarine particle populations using ADV, OBS and LISST, *Cont. Shelf Res.*, *22*(11–13), 1867–1886, doi:10.1016/S0278-4343(02)00043-2.

Ganju, N. K., D. H. Schoellhamer, M. C. Murrell, J. W. Gartner, and S. A. Wright (2006), Constancy of the relation between floc size and density in San Francisco Bay, in *Estuarine and Coastal Fine Sediment Dynamics - INTERCOH 2003*, edited by J. P. Maa, L. H. Sanford, and D. H. Schoellhamer, pp. 75–91, Elsevier, Amsterdam, Netherlands.

Gardner, W. D., et al. (2001), Optics, particles, stratification, and storms on the New England continental shelf, *J. Geophys. Res.*, *106*, 9473–9497, doi:10.1029/2000JC900161.

Gonzalez, R. C., R. E. Woods, and S. L. Eddins (2004), *Digital Image Processing Using MATLAB*, 609 pp., Prentice Hall, Upper Saddle River, N. J.

Grant, W. D., and O. S. Madsen (1986), The continental-shelf bottom boundary layer, *Annu. Rev. Fluid Mech.*, *18*, 265–305, doi:10.1146/annurev.fl.18.010186.001405.

Guillen, J., A. Palanques, P. Puig, X. D. De Madron, and F. Nyffeler (2000), Field calibration of optical sensors for measuring suspended sediment concentration in the western Mediterranean, *Sci. Mar.*, *64*(4), 427–435.

Hall, I. R., S. Schmidt, I. N. McCave, and J. L. Reyss (2000), Particulate matter distribution and Th-234/U-238 disequilibrium along the Northern Iberian Margin: Implications for particulate organic carbon export, *Deep Sea Res., Part I*, *47*(4), 557–582, doi:10.1016/S0967-0637(99)00065-5.

Harris, P. T., and P. E. O'Brien (1998), Bottom currents, sedimentation and ice-sheet retreat facies successions on the Mac Robertson shelf, East Antarctica, *Mar. Geol.*, *151*(1–4), 47–72, doi:10.1016/S0025-3227(98)00047-4.

Hatcher, A., P. Hill, and J. Grant (2001), Optical backscatter of marine flocs, *J. Sea Res.*, *46*(1), 1–12, doi:10.1016/S1385-1101(01)00066-1.

Hill, P. S., C. R. Sherwood, R. W. Sternberg, and A. R. M. Nowell (1994), In-situ measurements of particle settling velocity on the northern California continental shelf, *Cont. Shelf Res.*, *14*(10–11), 1123–1137, doi:10.1016/0278-4343(94)90031-0.

Hill, P. S., J. P. Syvitski, E. A. Cowan, and R. D. Powell (1998), In situ observations of floc settling velocities in Glacier Bay, Alaska, *Mar. Geol.*, *145*(1–2), 85–94, doi:10.1016/S0025-3227(97)00109-6.

Hill, P. S., et al. (2007), Sediment delivery to the seabed on continental margins, in *Continental Margin Sedimentation: Transport to Sequence*, *Spec. Publ. 37*, edited by C. A. Nittrouer et al., pp. 49–99, Blackwell, Oxford, U. K.

Holdaway, G. P., P. D. Thorne, D. Flatt, S. E. Jones, and D. Prandle (1999), Comparison between ADCP and transmissometer measurements of suspended sediment concentration, *Cont. Shelf Res.*, *19*(3), 421–441, doi:10.1016/S0278-4343(98)00097-1.

Inthorn, M., V. Mohrholz, and M. Zabel (2006), Nepheloid layer distribution in the Benguela upwelling area offshore Namibia, *Deep Sea Res., Part I*, *53*(8), 1423–1438, doi:10.1016/j.dsr.2006.06.004.

Jago, C. F., and C. F. J. Bull (2000), Quantification of errors in transmissometer-derived concentration of suspended particulate matter in the coastal zone: Implications for flux determinations, *Mar. Geol.*, *169*(3–4), 273–286, doi:10.1016/S0025-3227(00)00079-7.

Karageorgis, A. P., W. D. Gardner, D. Georgopoulos, A. V. Mishonov, E. Krasakopoulou, and C. Anagnostou (2008), Particle dynamics in the Eastern Mediterranean Sea: A synthesis based on light transmission, PMC, and POC archives (1991–2001), *Deep Sea Res., Part I*, *55*(2), 177–202, doi:10.1016/j.dsr.2007.11.002.

Khelifa, A., and P. S. Hill (2006), Models for effective density and settling velocity of flocs, *J. Hydraul. Res.*, *44*(3), 390–401, doi:10.1080/00221686.2006.9521690.

Law, B. A., P. S. Hill, T. G. Milligan, K. J. Curran, P. L. Wiberg, and R. A. Wheatcroft (2008), Size sorting of fine-grained sediments during erosion: Results from the western Gulf of Lions, *Cont. Shelf Res.*, *28*(15), 1935–1946, doi:10.1016/j.csr.2007.11.006.

Li, X. Y., and B. E. Logan (1997), Collision frequencies of fractal aggregates with small particles by differential sedimentation, *Environ. Sci. Technol.*, *31*(4), 1229–1236, doi:10.1021/es960771w.

Logan, B. E., and D. B. Wilkinson (1990), Fractal geometry of marine snow and other biological aggregates, *Limnol. Oceanogr.*, *35*(1), 130–136, doi:10.4319/lo.1990.35.1.0130.

Loisel, H., X. Meriaux, J.-F. Berthon, and A. Poteau (2007), Investigation of the optical backscattering to scattering ratio of marine particles in relation to their biogeochemical composition in the eastern English Channel and southern North Sea, *Limnol. Oceanogr.*, *52*(2), 739–752, doi:10.4319/lo.2007.52.2.0739.

Maggi, F. (2007), Variable fractal dimension: A major control for floc structure and flocculation kinematics of suspended cohesive sediment, *J. Geophys. Res.*, *112*, C07012, doi:10.1029/2006JC003951.

Manning, A. J., S. J. Bass, and K. R. Dyer (2006), Floc properties in the turbidity maximum of a mesotidal estuary during neap and spring tidal conditions, *Mar. Geol.*, *235*(1–4), 193–211, doi:10.1016/j.margeo.2006.10.014.

McCave, I. N. (1983), Particulate size spectra, behavior, and origin of nepheloid layers over the Nova Scotian continental rise, *J. Geophys. Res.*, *88*(C12), 7647–7666, doi:10.1029/JC088iC12p07647.

McCave, I. N. (1984), Size spectra and aggregation of particles in the deep ocean, *Deep Sea Res., Part A*, *31*(4), 329–352.

Mikkelsen, O. A. (2002), Variation in the projected surface area of suspended particles: Implications for remote sensing assessment of TSM, *Remote Sens. Environ.*, *79*(1), 23–29, doi:10.1016/S0034-4257(01)00235-8.

Mikkelsen, O. A., and M. Pejrup (2000), In situ particle size spectra and density of particle aggregates in a dredging plume, *Mar. Geol.*, *170*(3–4), 443–459, doi:10.1016/S0025-3227(00)00105-5.

Mikkelsen, O. A., T. G. Milligan, P. S. Hill, and D. Moffatt (2004), INSSECT - An instrumented platform for investigating floc properties close to the seabed, *Limnol. Oceanogr. Methods*, *2*, 226–236.

Mikkelsen, O. A., P. S. Hill, T. G. Milligan, and R. J. Chant (2005), In situ particle size distributions and volume concentrations from a LISST-100 laser particle sizer and a digital floc camera, *Cont. Shelf Res.*, *25*(16), 1959–1978, doi:10.1016/j.csr.2005.07.001.

Mikkelsen, O. A., P. S. Hill, and T. G. Milligan (2006), Single-grain, microfloc and macrofloc volume variations observed with a LISST-100 and a digital floc camera, *J. Sea Res.*, *55*(2), 87–102, doi:10.1016/j.seares.2005.09.003.

Mikkelsen, O. A., K. J. Curran, P. S. Hill, and T. G. Milligan (2007), Entropy analysis of in situ particle size, *Estuarine Coastal Shelf Sci.*, *72*(4), 615–625, doi:10.1016/j.ecss.2006.11.027.

Milligan, T. G., P. S. Hill, and B. A. Law (2007), Flocculation and the loss of sediment from the Po River plume, *Cont. Shelf Res.*, *27*(3–4), 309–321, doi:10.1016/j.csr.2006.11.008.

Moore, K. A., R. L. Wetzel, and R. J. Orth (1997), Seasonal pulses of turbidity and their relations to eelgrass (Zostera marina L.) survival in an estuary, *J. Exp. Mar. Biol. Ecol.*, *215*(1), 115–134, doi:10.1016/S0022-0981(96)02774-8.

Nikora, V., J. Aberle, and M. Green (2004), Sediment flocs: Settling velocity, flocculation factor, and optical backscatter, *J. Hydraul. Eng.*, *130*(10), 1043–1047, doi:10.1061/(ASCE)0733-9429(2004)130:10(1043).

Orbach, R. (1986), Dynamics of fractal networks, *Science*, *231*(4740), 814–819, doi:10.1126/science.231.4740.814.

Otsu, N. (1979), A threshold selection method from gray-level histograms, *IEEE Trans. Syst. Man Cybern.*, *9*(1), 62–66, doi:10.1109/TSMC.1979.4310076.

Peterson, R. L. (1977), A study of suspended particulate matter: Arctic Ocean and northern Oregon continental shelf, Ph.D thesis, Oregon State Univ., Corvallis.

Pierson, D. C., and G. A. Weyhenmeyer (1994), High resolution measurements of sediment resuspension above an accumulation bottom in a stratified lake, *Hydrobiologia*, *284*(1), 43–57, doi:10.1007/BF00005730.

Piskozub, J., D. Stramski, E. Terrill, and W. K. Melville (2004), Influence of forward and multiple light scatter on the measurement of beam attenuation in highly scattering marine environments, *Appl. Opt.*, *43*(24), 4723–4731, doi:10.1364/AO.43.004723.

Puig, P., A. Palanques, J. Guillen, and E. Garcia-Ladona (2000), Deep slope currents and suspended particle fluxes in and around the Foix submarine canyon (NW Mediterranean), *Deep Sea Res., Part I*, *47*(3), 343–366, doi:10.1016/S0967-0637(99)00062-X.

Santschi, P. H., J. J. Lenhart, and B. D. Honeyman (1997), Heterogeneous processes affecting trace contaminant distribution in estuaries: The role of natural organic matter, *Mar. Chem.*, *58*(1–2), 99–125, doi:10.1016/S0304-4203(97)00029-7.

Sheldon, R. W. (1972), Size separation of marine seston by membrane and glass-fiber filters, *Limnol. Oceanogr.*, *17*(3), 494–498, doi:10.4319/lo.1972.17.3.0494.

Sherwood, C. R., B. Butman, D. A. Cacchione, D. E. Drake, T. F. Gross, R. W. Sternberg, P. L. Wiberg, and A. J. Williams (1994), Sediment transport events on the northern California continental shelf during the 1990–1991 STRESS Experiment, *Cont. Shelf Res.*, *14*(10–11), 1063–1099, doi:10.1016/0278-4343(94)90029-9.

Smith, D. G., G. F. Croker, and K. McFarlane (1995), Human perception of water appearance. 1. Clarity and colour for bathing and aesthetics, *N. Z. J. Mar. Freshw. Res.*, *29*(1), 29–43, doi:10.1080/00288330.1995.9516637.

Sternberg, R. W., I. Berhane, and A. S. Ogston (1999), Measurement of size and settling velocity of suspended aggregates on the northern California continental shelf, *Mar. Geol.*, *154*(1–4), 43–53, doi:10.1016/S0025-3227(98)00102-9.

Syvitski, J. P. M., K. W. Asprey, and K. W. G. Leblanc (1995), In-situ characteristics of particles settling within a deep-water estuary, *Deep Sea Res., Part II*, *42*(1), 223–256, doi:10.1016/0967-0645(95)00013-G.

Traykovski, P., R. J. Latter, and J. D. Irish (1999), A laboratory evaluation of the laser in situ scattering and transmissometery instrument using natural sediments, *Mar. Geol.*, *159*(1–4), 355–367, doi:10.1016/S0025-3227(98)00196-0.

Trowbridge, J., and S. Elgar (2003), Spatial scales of stress-carrying nearshore turbulence, *J. Phys. Oceanogr.*, *33*(5), 1122–1128, doi:10.1175/1520-0485(2003)033<1122:SSOSNT>2.0.CO;2.

van de Hulst, H. C. (1981), *Light Scattering by Small Particles*, 470 pp., Dover, New York.

Wells, J. T., and S. Y. Kim (1991), The relationship between beam transmission and concentration of suspended particulate material in the Neuse River estuary, North Carolina, *Estuaries*, *14*(4), 395–403, doi:10.2307/1352264.

Wiberg, P. L., D. E. Drake, and D. A. Cacchione (1994), Sediment resuspension and bed armoring during high bottom stress events on the northern California inner continental shelf: Measurements and predictions, *Cont. Shelf Res.*, *14*(10–11), 1191–1219, doi:10.1016/0278-4343(94)90034-5.

Winterwerp, J. C., and W. G. M. van Kesteren (2004), Introduction to the physics of cohesive sediment in the marine environment, *Develop. Sedimentol.*, *56*, 466 pp.

Xu, F. H., D. P. Wang, and N. Riemer (2008), Modeling flocculation processes of fine-grained particles using a size-resolved method: Comparison with published laboratory experiments, *Cont. Shelf Res.*, *28*(19), 2668–2677, doi:10.1016/j.csr.2008.09.001.

Yamasaki, A., H. Fukuda, R. Fukuda, T. Miyajima, T. Nagata, H. Ogawa, and I. Koike (1998), Submicrometer particles in Northwest Pacific coastal environments: Abundance, size, distribution, and biological origins, *Limnol. Oceanogr.*, *43*(3), 536–542, doi:10.4319/lo.1998.43.3.0536.

E. Boss, School of Marine Sciences, University of Maine, 458 Aubert Hall, Orono, ME 04469, USA.

P. S. Hill and J. P. Newgard, Department of Oceanography, Dalhousie University, 1355 Oxford St., Halifax, NS B3H 4J1, Canada. (paul.hill@dal.ca)

B. A. Law and T. G. Milligan, Fisheries and Oceans Canada, Bedford Institute of Oceanography, PO Box 1006, Dartmouth, NS B2Y 4A2, Canada.